Academic Journal of Science and Technology
ISSN: 2771-3032 | Vol. 15, No. 2, 2025

Inter-turn Short Circuit Fault Diagnosis for PMSMs Based on a Novel Search Coil

Caixia Gao[1], Weifeng Liu[2,*]

[1] School of Electrical Engineering and Automation, Henan Polytechnic University, Jiaozuo 454000, China
[2] School of Electrical Engineering and Automation, Henan Polytechnic University, Jiaozuo 454000, China
[*] Corresponding author

Abstract: Permanent magnet synchronous motors (PMSMs) may suffer from inter-turn short-circuit faults (ISFs) during their operation, which brings great challenges to the fault diagnosis of PMSMs and results in insufficient research on ISF diagnosis. To solve this problem, this paper proposes a novel search coil (SC) arrangement method for ISF diagnosis of PMSM. With the proposed configuration of SCs, it only needs to be installed on specific stator teeth. Then, a mathematical model of SC is developed, which serves as a basis for future investigations into fault characteristics using the novel SCs. Furthermore, by examining the time-domain characteristics of the search coil group (SCG), the time-domain energy of the SCG voltage is proposed as a fault diagnostic indicator. The finite element method (FEM) and experiments validate the correctness and effectiveness of the proposed method.

Keywords: Permanent magnet synchronous motor, Inter-turn short-circuit fault, Search coil, Finite element.

1. Introduction

Permanent magnet synchronous motors (PMSMs) are used in many industrial applications owing to their advantages such as high efficiency, and higher power density [1-3]. Nevertheless, when exposed to harsh conditions such as high temperatures, and humidity, inter-turn short-circuit faults (ISFs) may arise [4-5]. These faults not only degrade motor performance but can even trigger catastrophic system failures, leading to substantial economic losses and safety risks [6-7]. Accurate diagnosis of ISFs is therefore critical for enhancing motor reliability, operational safety, and cost-effectiveness. As such, investigating effective ISF diagnosis methods for PMSMs carries significant practical importance.

According to the approaches for acquiring ISF signals, the diagnostic methods can be classified into those based on external motor signals and those based on internal motor signals.

Diagnostic methods based on external motor signals are the most widely applied. These methods use directly measurable signals from the motor's exterior, such as voltage[8], current[9], electromagnetic torque[10], vibration, and noise[11], as the basis for analysis. Fault-characteristic information is extracted through signal processing techniques. However, this approach relies heavily on a large volume of historical data, and its diagnostic accuracy is susceptible to data noise.

To address these limitations, researchers have proposed diagnostic methods based on internal motor signals. The magnetic field, serving as the bridge for energy conversion between electrical and mechanical forms in motors, contains critical information about the motor's health or ISF conditions. ISFs cause magnetic field distortion, and monitoring changes in the magnetic field before and after a fault enables fault diagnosis. Thus, some scholars use electromagnetic signals as characteristic signals for ISFs. For example, Reference [12] installs tunneling sensors on the motor housing to monitor the leakage flux outside the stator yoke and realizes fault diagnosis by comparing leakage flux differences before and after the fault. Reference [13] employs eight fluxgate sensors on the motor housing to monitor leakage flux and proposes a diagnosis method based on the third harmonic of leakage flux. Reference [14] uses Hall sensors on the end cover to detect changes in leakage flux and identifies faults by comparing peak value variations of leakage flux before and after the fault. Although ISF diagnosis methods based on leakage flux have low invasiveness and are unaffected by motor topology, the weak leakage flux signals are prone to external noise interference, which degrades diagnostic accuracy.

To mitigate the impact of external noise on diagnostic accuracy, researchers have developed methods using search coils (SCs) installed inside the motor. References [15-16] achieve ISF diagnosis by mounting SCs on each stator tooth. Specifically, Reference [15] analyzes the harmonic component changes of tooth flux before and after the fault and uses high-order harmonics as diagnostic criteria, while Reference [16] uses low-frequency components of the SC voltage as the basis for diagnosis. However, installing SCs on each stator tooth increases motor invasiveness and elevates manufacturing complexity and production costs. To reduce invasiveness, Reference [17] installs SCs on specific stator teeth and monitors voltage variations in these coils before and after faults to diagnose ISFs. Further reducing invasiveness, Reference [18] places six exploratory coils with a 60° spatial difference on the stator and realizes fault diagnosis by analyzing high-order harmonic changes in the SC voltages before and after the fault. However, this method requires storing a large amount of healthy state data.

To overcome the limitations of existing ISF diagnosis methods for PMSMs, this paper presents a novel ISF diagnosis approach based on a specially designed SC configuration. By reverse-series connecting signals collected from adjacent SCs within the same stator branch, a search coil group (SCG) is formed. Unlike traditional SCs installed on each stator tooth, the SCG generates a unique voltage waveform under each fault condition, enabling effective fault diagnosis. The proposed diagnostic algorithm, built on constructed fault diagnosis indices, is straightforward and requires minimal computational resources. Moreover, it

supports online diagnosis, eliminating the need for storing large datasets. Both the finite element method (FEM) and experimental have verified the correctness and effectiveness of the proposed method for ISF diagnosis.

2. Novel Search Coil Mechanism Analysis

This section presents a criterion for installing SCs to diagnose ISFs in PMSMs. A mathematical model is then developed to analyze the SC voltage under both healthy and faulty conditions. Finally, the correctness and effectiveness of the proposed method are verified via FEM simulations, and the variation patterns of the SC voltage during ISF occurrence are systematically analyzed.

(1) Novel search coil topology design

Coils adjacent to each other in the same branch are defined as a coil group, which can be classified into two structures, as shown in Fig 1. A coil group consisting of two coils is referred to as a Type-I unit, while a three-coil group is designated as a Type-II unit. The installation positions of the SCs in both types of coil groups are also illustrated in Fig 1, and the number of SCs can be calculated using Equations (1) and (2).

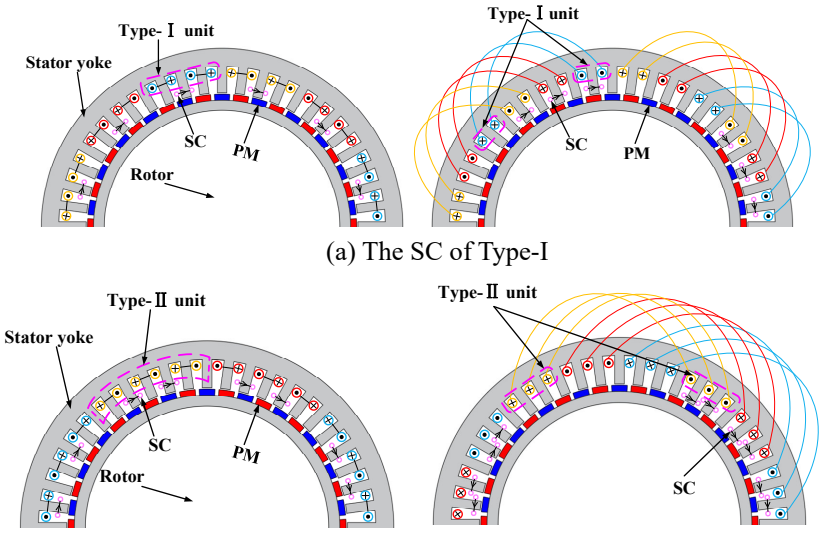

(a) The SC of Type-I

(b) The SC of Type-II

Figure 1. Schematic diagram of SC Topology

$$n_{coil} = 2n_{\mathrm{I}} + 3n_{\mathrm{II}} \quad (1)$$

$$n_{SC} = n_{\mathrm{I}} + 2n_{\mathrm{II}} \quad (2)$$

where ncoil, n Ⅰ, and n Ⅱ are the number of coils, Type-I units, and Type-II units in the coil group, respectively. nSC is the number of SCs installed.

To minimize the invasiveness of SCs on the motor, it is necessary to select an appropriate scheme to reduce the number of SCs. For example, calculations based on Equations (1) and (2) show that for a coil group consisting of six coils, three Type-I SCs can be installed, or four Type-II SCs. Thus, choosing the Type-I SC installation method can effectively reduce invasiveness.

As shown in Fig.2, a PMSM with *m* coils in each branch (m=1, 2, 3…) as an example, where *Xi* denotes *i*th coil of phase *X* in the PMSM (*X*=A, B, C； *i*=1, 2, 3…). SC_{XYo} represents the SC between coil *Xo* and *X*(*o*+1), where *Y* indicates the SC type (*Y*=1 represents Type-I SC. Y=2 represents Type- II SC. *O*=*i*, *j*=1, 2, 3…).

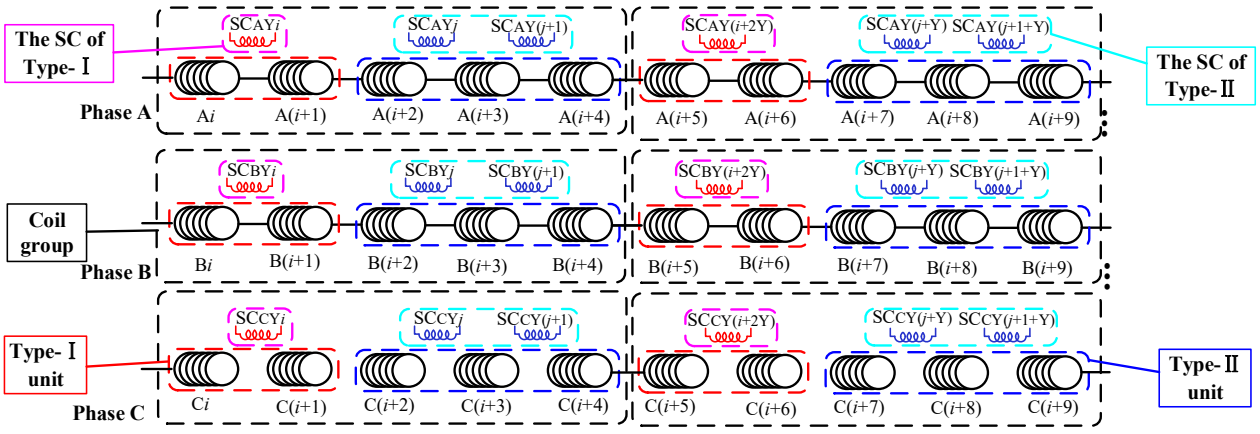

Figure 2. The schematic diagram of the SC arrangement

(2) Mathematical modeling for search coil voltage

Based on the above-mentioned SC arrangement, to achieve online ISF diagnosis of PMSMs, this section takes a 48-slot/44-pole surface-mounted PMSM as an example. By subtracting the voltage acquired from two specific SCs, a SCG voltage is formed, and the construction schematic of the SCG is shown in Fig 3.

As described in Reference [19], the SC voltage under health can be expressed as.

$$\begin{bmatrix} e_{scA1o} \\ e_{scB1o} \\ e_{scC1o} \end{bmatrix} = j2\pi f \begin{bmatrix} M_{A1o-A} & M_{A1o-B} & M_{A1o-C} \\ M_{B1o-A} & M_{B1o-B} & M_{B1o-C} \\ M_{C1o-A} & M_{C1o-B} & M_{C1o-C} \end{bmatrix} \frac{d}{dt} \begin{bmatrix} i_A \\ i_B \\ i_C \end{bmatrix} + N_C \begin{bmatrix} \phi_{A1o} \\ \phi_{B1o} \\ \phi_{C1o} \end{bmatrix} \quad (3)$$

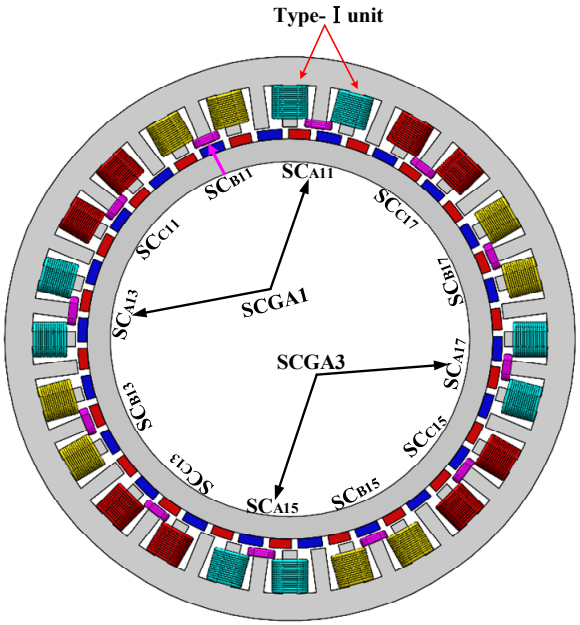

Figure 3. The schematic diagram of surface-mounted PMSM

$$\begin{cases} M_{A1o-A} = M_{s1} + M_{r1}\cos(2\theta) \\ M_{B1o-B} = M_{s1} + M_{r1}\cos(2\theta + 2\pi/3) \\ M_{C1o-C} = M_{s1} + M_{r1}\cos(2\theta - 2\pi/3) \\ M_{C1o-A} = -M_{A1o-C} = M_{s2} + M_{r2}\cos(2\theta + 2\pi/3) \\ M_{A1o-B} = -M_{B1o-A} = M_{s2} + M_{r2}\cos(2\theta - 2\pi/3) \\ M_{B1o-C} = -M_{C1o-B} = M_{s2} + M_{r2}\cos(2\theta) \end{cases} \quad (4)$$

$$\begin{cases} \phi_{A1o} = \phi_r \cos(\theta) \\ \phi_{B1o} = \phi_r \cos(\theta + 2\pi/3) \\ \phi_{C1o} = \phi_r \cos(\theta - 2\pi/3) \end{cases} \quad (5)$$

$$\theta = 2\pi f + \varphi \quad (6)$$

where e_{SCX1o} is the voltage of SC_{X1o}. $M_{X1o\text{-}X}$ represents the mutual inductance between SC_{X1o} and X phase winding. i_X is the currents of X phase winding. M_{s1} and M_{s2} are the average components between the phase windings and their corresponding SCG, as well as non-corresponding SCG. M_{r1} and M_{r2} are amplitude components between the phase windings and their corresponding SCG, as well as non-corresponding SCG. φ_{X1o} is the rotor magnetic flux of SC_{X1o}. Nc is the turn of SC. f is the power supply frequency, φ is the initial phase angle. φ_r is the amplitude of the magnetic flux of SC_{X1o}.

When the PMSM is under healthy cases, the SCG voltage can be expressed as.

$$\begin{bmatrix} e_{GA1o-H} \\ e_{GB1o-H} \\ e_{GC1o-H} \end{bmatrix} = \begin{bmatrix} e_{A1o-H} \\ e_{B1o-H} \\ e_{C1o-H} \end{bmatrix} - \begin{bmatrix} e_{A1(o+2)-H} \\ e_{B1(o+2)-H} \\ e_{C1(o+2)-H} \end{bmatrix} = \begin{bmatrix} 0 \\ 0 \\ 0 \end{bmatrix} \quad (7)$$

where $e_{GX1o\text{-H}}$ is the voltage of the SCG_{X1o} under healthy cases. $e_{X1o\text{-H}}$, and $e_{X1(o+2)\text{-H}}$ is the voltage of SC in health conditions. As shown in Fig.3, Due to the electrical angle difference of $m \cdot 180°$ between adjacent SCs, the voltage across the SCG is zero under healthy conditions.

When an ISF occurs in phase A, the SCG voltage can be expressed as.

$$\begin{bmatrix} e_{GA1o-I} \\ e_{GB1o-I} \\ e_{GC1o-I} \end{bmatrix} = \begin{bmatrix} e_{A1o-I} \\ e_{B1o-I} \\ e_{C1o-I} \end{bmatrix} - \begin{bmatrix} e_{A1(o+2)-I} \\ e_{B1(o+2)-I} \\ e_{C1(o+2)-I} \end{bmatrix} = j2\pi f \eta \begin{bmatrix} k_{o1}M_{A1o} \\ k_{o2}M_{B1o} \\ k_{o3}M_{C1o} \end{bmatrix} i_f \quad (8)$$

$$i_f = \frac{R_f i_A - \eta N_s \phi_{r1} - j2\pi f[(2\eta - 1)]L_{AA} i_A + M_{AB} i_B + M_{AC} i_C}{R_f + \eta R_s + j2\pi f \eta^2 L_{AA}} \quad (9)$$

$$\eta = \frac{N_f}{nN_s} \times 100\% \quad (10)$$

$$\begin{cases} L_{AA} = M_{s3} + M_{r3}\cos(2\theta) \\ M_{AB} = M_{s4} + M_{r4}\cos(2\theta - 2\pi/3) \\ M_{AC} = M_{s4} + M_{r4}\cos(2\theta + 2\pi/3) \end{cases} \quad (11)$$

where $e_{GX1o\text{-I}}$ is the SCG voltage under ISF conditions. $SC_{X1o\text{-I}}$ and $SC_{X1(o+2)\text{-I}}$ are the SC voltage under ISF conditions. k_{o1}、k_{o2} and k_{o3} the mutual inductance correction coefficients which are $0 < k_{om} < 1$. i_f, R_f, R_s are the short-circuit current, short-circuit resistance and phase resistance. N_f, N_s are the number of short-circuit turns and coil turns. n is the number of coils of phase A. η is the short-circuit ratio. L_{AA} is the self-inductance of phase A. M_{AB} is the mutual-inductance between phase A and phase B, M_{AC} is the mutual-inductance between phase A and phase C. φ_{r1} is the rotor magnetic flux in the faulty phase, and φ_1 is the initial phase angle of the magnetic flux in the faulty phase.

Considering the influence of magnetic pole shape, slot effect, and PM working point on the calculation accuracy of the model, this paper uses the FEM to calculate M_{s1}, M_{r1}, M_{s2}, M_{r2}, φr, k_{om}、M_{s3}、M_{s4}、M_{r3}、M_{r4} and φ.

(3) Correctness verification of the mathematical model

To verify the developed mathematical model, a FEM model was constructed based on the parameters of a 48-slot/44-pole PMSM available in the laboratory. The main parameters of this PMSM are presented in Table 1.

Table 1. The key parameters of PMSM

Items	Values	Unit
Out diameter of stator	270	mm
Inner diameter of stator	203	mm
Air-gap length	0.9	mm
Wire diameter of winding	1	mm
Thickness of PM	4.5	mm
Pole-arc coefficient	0.73	/
Axial length	100	mm
Rated power	1.5	kW
Rated speed	180	rpm
Rated current	4	Arms
Number of phases	3	/
Number of coils	24	/
Coil turns	70	/
Parallel-circuits per phase	1	/
Slot-pole combination	48-44	/
Rated frequency	66	Hz
Magnets type	NdFeB	
Magnet remanent magnetic flux density	1.35	T
Magnet width	11	mm
Magnet length	100	mm

The healthy and ISF condition are presented FEM and mathematical model, and listed in Table 2.

Table 2. The healthy and ISF condition

Fault condition	Fault position/degree
Healthy	/
ISF	Coil A2/12.5%

The calculation results of the FEM and the mathematical model under rated operating conditions are shown in Fig.4

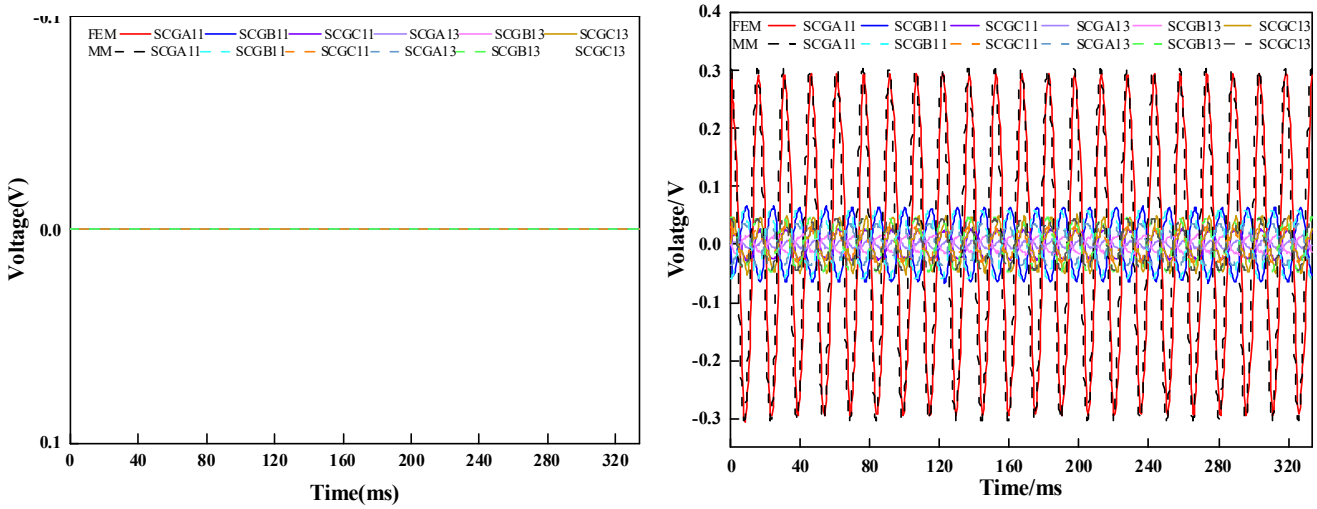

(a) The calculation result in healthy (b) The calculation result under ISF

Figure 4. The calculation result of FEM and mathematical model

As shown in Fig. 4, the FEM calculation results under both healthy and ISF conditions exhibit good agreement with the mathematical model predictions, with maximum errors of 0% and 2.29%, respectively. These errors are attributed to the neglect of factors such as magnetic circuit saturation and iron losses during the modeling process.

As shown in Fig.4(a), when the PMSM operates in healthy conditions, the voltage of each SCG remains at 0. It can be seen from Fig.4(b) that during an ISF, the SCG closest to the faulty coil exhibits the highest amplitude, while the amplitudes of other SCGs decrease progressively as their spatial distance from the fault location increases.

3. Fault Diagnosis Method for PMSM Based on Novel-type Search Coil

As shown in Figure 4, there is a significant difference in the SCG voltage between healthy and ISF. This indicates that the voltage waveform of the SCG contains critical information about the motor's operating state. Therefore, this section constructs a fault diagnosis indicator using the energy signal of the SCG voltage waveform within a stable

mechanical cycle, which can be expressed as.

$$F_{X1o} = \sum_{i=1}^{N} S_i \tag{12}$$

To analyze the effect of operating conditions on the sensitivity of fault diagnosis indicators, this study evaluates these indicators across a spectrum of motor speeds and loads.

Fig.5 shows the fault diagnosis indicators under varying speed conditions.

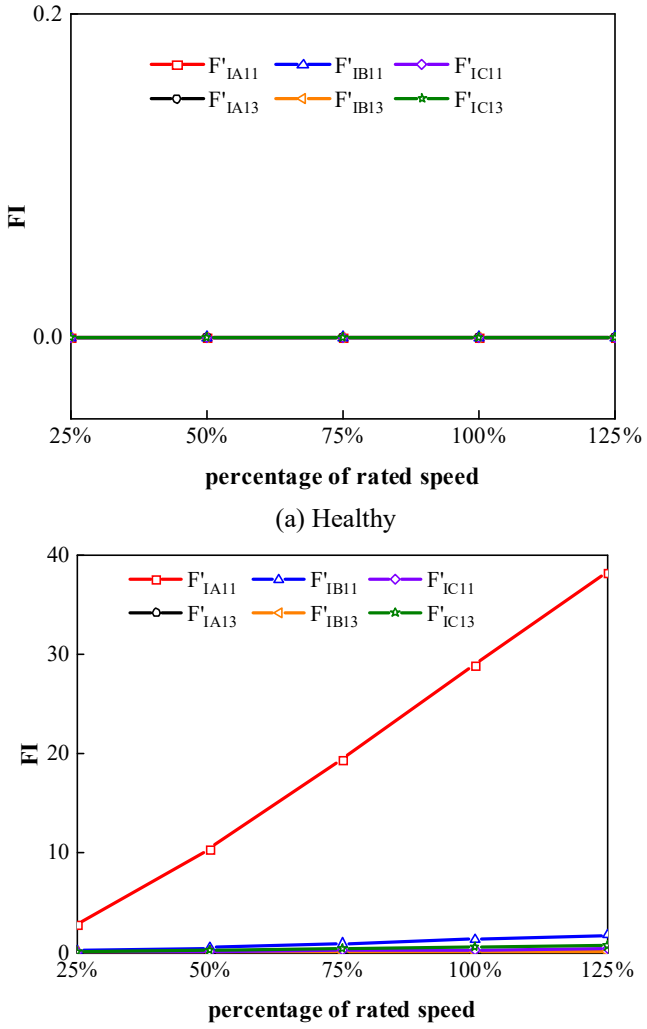

(a) Healthy

(b) ISF

Figure 5. The effect of varying speeds on fault diagnosis indicators

As shown in Fig. 5, the fault diagnosis indicators for the healthy PMSM remain zero across all tested speeds, whereas those under faulty conditions exhibit non-zero values. This demonstrates that the proposed indicator enables accurate detection of motor faults at any speed.

Fig.6 shows fault diagnosis indicators under varying load conditions.

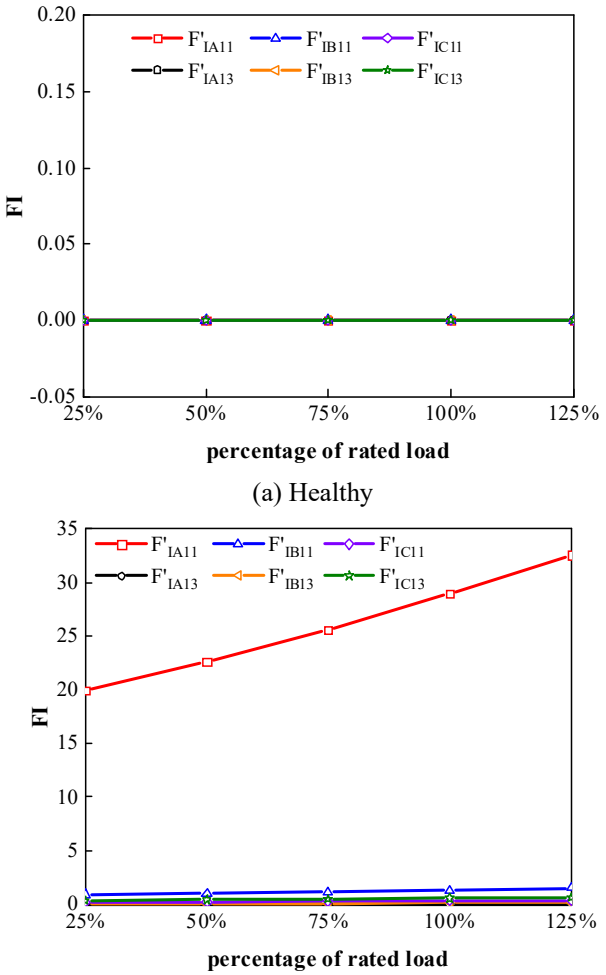

(a) Healthy

(b) ISF

Figure 6. The effect of varying speeds on fault diagnosis indicators.

As shown in Fig. 6, the fault diagnosis indicators for the healthy PMSM remain zero across all tested speeds, whereas those under faulty conditions exhibit non-zero values. This demonstrates that the proposed indicator enables accurate detection of motor faults at any load.

Therefore, the proposed fault diagnosis indicator can accurately identify whether an ISF has occurred in thePMSM.

The ISF diagnostic algorithm is shown in Fig 7, and the specific diagnostic steps are as follows.

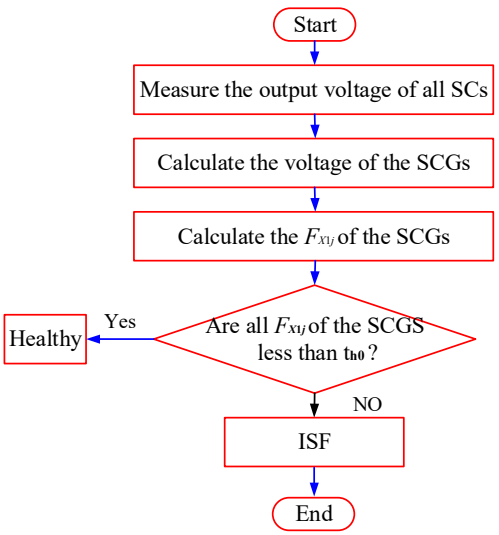

Figure 7. Fault diagnosis algorithm for PMSM

1) Signal Acquisition. Measure the voltages of all SCs over one rotor rotation using a data acquisition card, and transfer the signals to a computer, and simultaneously, record the motor speed and load torque using a torque transducer.

2) Data processing. Apply a low-pass filter in MATLAB to suppress noise in the measured SC voltages.

3) SCG voltage calculate. Compute the SCG voltage by subtracting the filtered SC voltages according to the predefined SCG arrangement.

4) Fault diagnosis. Set the threshold parameter (th0), and Compare the calculated SCG energy indicator with th_0 to determine the presence of ISFs.

4. Experimental Verification

In order to verify the correctness of the proposed method, an experimental platform was set up, as shown in Fig. 8, and specifications of the prototype used in this experiment are listed in Table 1. The driver drives the healthy or faulty prototype respectively, while another motor operates as a load. The torque transducer to measure the speed and torque. The SCs with is 0.5 mm and five turns per coil are installed in test prototype. Each SC has one terminal connected to an NI data acquisition card and the other grounded. The acquisition card collects data and transfers it to a computer by USB, while an oscilloscope connected in parallel with the SC to visually display the induced electromotive forces. To simulate an ISF, a short-circuit resistor is connected in parallel with the target coil sub-unit.

Fig.9 shows the SCG voltage waveforms of the motor with healthy under rated condition.

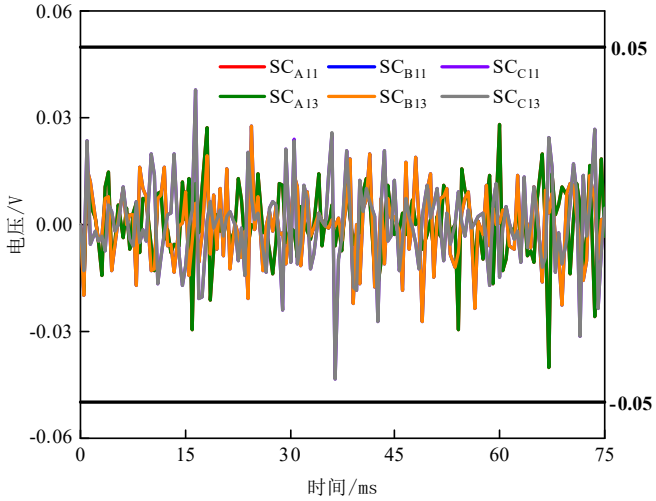

Figure 9. The SCG voltage under healthy state.

As shown in Fig.9, the SCGs voltage are extremely weak. Through calculation, th_0 can be set to 0.002.

Table 3 shows the ISF conditions preset on the prototype.

Table 3. The ISF conditions preset on the prototype

ISF condition	Short-circuit position	R_f(mΩ)
	A1 01~35	10

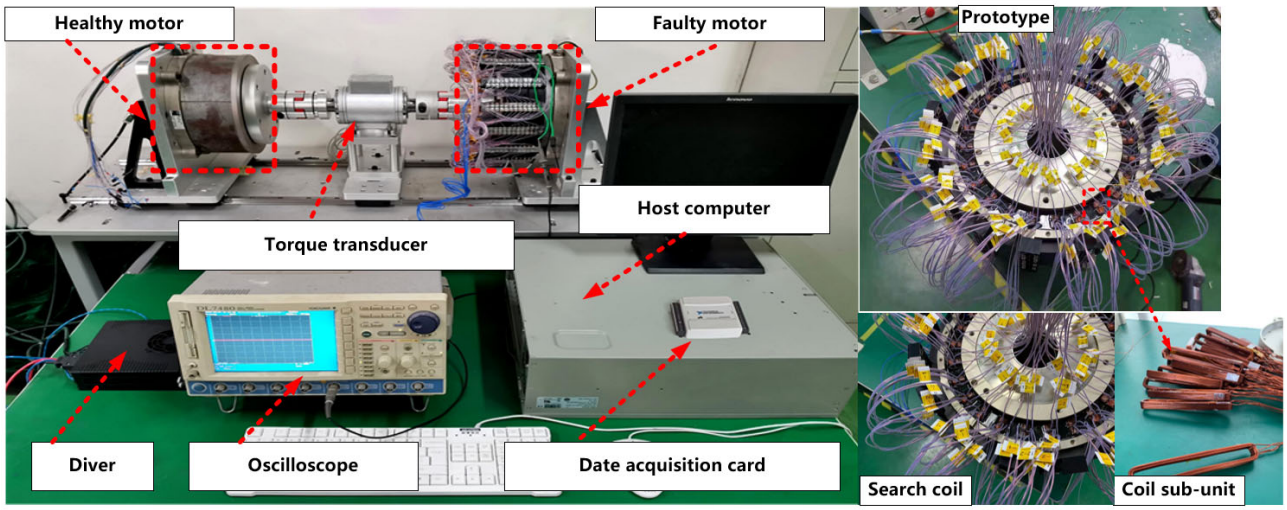

Figure 8. Experiment setup

Fig 10 shown the SCG voltage waveforms of the motor with ISF under rated condition.

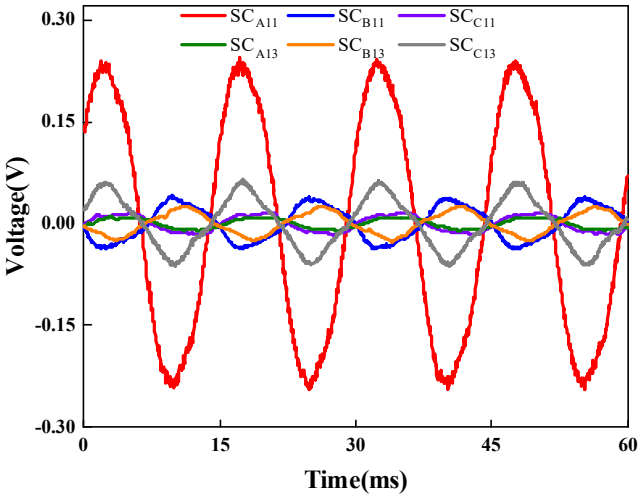

Figure 10. The SCG voltage under ISF

The diagnosis indicators for the ISF are shown in Table 4.

Table 4. The diagnosis indicators for healthy and IS

diagnosis indicator	Healthy	ISF
F_{A11}	0.0013	186.3
F_{B11}	0.0013	4.064
F_{C11}	0.0013	0.851
F_{A13}	0.0013	0.337
F_{B13}	0.0013	1.643
F_{C13}	0.0013	9.244

As shown in Table 4, when an ISF occurs, the diagnosis indicators can accurately detect the operating state of PMSM.

5. Conclusion

To realize ISF diagnosis for PMSMs, this study presents a novel SC configuration for PMSM. Both FEM and experiment validation confirm the correctness and effectiveness of the proposed method.

1. The newly proposed SC structure only requires installation on specific stator teeth, which not only reduces the number of SCs required but also minimizes the invasiveness of the motor..

2. A mathematical model of SC for ISF analysis was established to examine voltage variation patterns under faulty conditions. The comparative analysis with the FEM verifies the accuracy and correctness of the established model, providing a solid theoretical foundation for the development of ISF diagnostic indicators.

3. The proposed method demonstrates broad applicability, suitable for both concentrated-winding and distributed-winding PMSMs. Additionally, it exhibits strong robustness across different operating conditions.

References

[1] Y. Qi, E. Bostanci, V. Gurusamy, et al. A Comprehensive Analysis of Short-Circuit Current Behavior in PMSM Interturn Short-Circuit Faults [J]. IEEE Transactions on Power Electronics, 2018, 33(12): 10784-10793.

[2] F. Huang et al. Demagnetization Fault Diagnosis of Permanent Magnet Synchronous Motors Using Magnetic Leakage Signals [J]. IEEE Transactions on Industrial Informatics, 2023, 19 (4): 6105-6116.

[3] L. Zezula, M. Kozovsky and P. Blaha. Diagnostics of Interturn Short Circuits in PMSMs With Online Fault Indicators Estimation [J]. IEEE Transactions on Industrial Electronics, 2024 71(11): 15001-15011.

[4] R. Hu, J. Wang, A. R. Mills, et al. Current-Residual-Based Stator Interturn Fault Detection in Permanent Magnet Machines [J]. IEEE Transactions on Industrial Electronics, 2021, 68(1): 59-69.

[5] K. H. Baruti, C. Li, F. Erturk, et al. Online Stator Inter-Turn Short Circuit Estimation and Fault Management in Permanent Magnet Motors [J]. IEEE Transactions on Energy Conversion, 2023 38(2): 1016-1027.

[6] S. Moon, H. Jeong, H. Lee, et al. Interturn Short Fault Diagnosis in a PMSM by Voltage and Current Residual Analysis With the Faulty Winding Model [J]. IEEE Transactions on Energy Conversion, 2018, 33(1): 190-198.

[7] V. Gurusamy, E. Bostanci, C. Li, et al. A Stray Magnetic Flux-Based Robust Diagnosis Method for Detection and Location of Interturn Short Circuit Fault in PMSM [J]. IEEE Transactions on Instrumentation and Measurement, 2021, 70: 1-11.

[8] Mazzoletti M. A, Bossio G. R, De Angelo C. H. Interturn short-circuit fault diagnosis in PMSM with partitioned stator windings [J]. IET Electric Power Applications, 2020, 14(12): 2301-2311.

[9] Zhang Xiaoke, Jiao Ningfei, Mao Shuai, et al. A Method for Estimating the Rotor Position of an Aviation Multistage Starter/Generator in Low-Speed Segment Based on Stator Direct Axis Current Point Sampling of the Exciter [J/OL]. Journal of Chinese Electrical Engineering, 2024.

[10] Zhao Jing, Guan Xiaoqing, Li Chenghai, et al. A Comprehensive Evaluation of Inter-Turn Short Circuit Faults in PMSM Used for Electric Vehicles [J]. IEEE Transactions on Intelligent Transportation Systems, 2021, 22(1): 611-621.

[11] He Yu-Ling, Xu Ming-Xing, Zhang Wen, et al. Impact of Stator Interturn Short Circuit Position on End Winding Vibration in Synchronous Generators [J]. IEEE Transactions on Energy Conversion, 2021, 36(2): 713-724.

[12] X. Liu, W. Miao, Q. Xu, et al., Inter-Turn Short-Circuit Fault Detection Approach for Permanent Magnet Synchronous Machines Through Stray Magnetic Field Sensing [J]. IEEE Sensors Journal, 2019, 19(18): 7844-7895.

[13] V. Gurusamy, E. Bostanci, C. Li, et al. A Stray Magnetic Flux-Based Robust Diagnosis Method for Detection and Location of Interturn Short Circuit Fault in PMSM [J].IEEE Transactions on Instrumentation and Measurement, 2021, 70: 1-11.

[14] G. Mirzaeva, K. Saadi. Advanced Diagnosis of Stator Turn-to-Turn Faults and Static Eccentricity in Induction Motors Based on Internal Flux Measurement [J]. IEEE Transactions on Industry Applications, 2018, 54(4): 3961-3970.

[15] Z. Chong, S. Huang, Y. Yang, et al. Inter-turn fault diagnosis of permanent magnet synchronous machine based on tooth magnetic flux analysis [J]. IET Electric Power Applications, 2018, 12(6): 837-844.

[16] T. Lee, K. Kim, J. Hur. Diagnosis technique using detection coil in BLDC motor with Interturn Fault [J]. IEEE Transactions on Magnetics, 2014, 50(2): 1-4.

[17] Chen Hao, Zhang Nan, Gao Caixia, et al. Method for Locating Short-Circuit Fault Short Circuit Loops in Permanent Magnet Synchronous Motors [J]. Journal of Electric Machines and Control, 2023, 27(3): 124-134.

[18] W. Huang, B. Du, T. Li, et al. Inter-turn Short-Circuit Fault Diagnosis of Interior Permanent Magnet Synchronous Motor for Electric Vehicle Based on Search Coil [J]. IEEE Transactions on Power Electronics, 2023, 38(2): 2506-2515.

[19] J. Zhao, X. Guan, C. Li, Q. Mou, et al. Comprehensive Evaluation of Inter-Turn Short Circuit Faults in PMSM Used for Electric Vehicles [J]. IEEE Transactions on Intelligent Transportation Systems, 2021, 22(1): 611-621.